Spatial correlations in polycarbonates: Neutron scattering and simulation

J. Eilhard, A. Zirkel, W. Tschöp, O. Hahn, K. Kremer, O. Schärpf, D. Richter, and U. Buchenau

Citation: The Journal of Chemical Physics **110**, 1819 (1999); doi: 10.1063/1.477889
View online: https://doi.org/10.1063/1.477889
View Table of Contents: http://aip.scitation.org/toc/jcp/110/3
Published by the American Institute of Physics

Articles you may be interested in

Molecular dynamics simulation study of nonconcatenated ring polymers in a melt. I. Statics
The Journal of Chemical Physics **134**, 204904 (2011); 10.1063/1.3587137

Dynamics of entangled linear polymer melts: A molecular-dynamics simulation
The Journal of Chemical Physics **92**, 5057 (1990); 10.1063/1.458541

Static and dynamic properties of large polymer melts in equilibrium
The Journal of Chemical Physics **144**, 154907 (2016); 10.1063/1.4946033

Fast equilibration protocol for million atom systems of highly entangled linear polyethylene chains
The Journal of Chemical Physics **144**, 154901 (2016); 10.1063/1.4946802

Sub-T_g dynamics in polycarbonate by neutron scattering and its relation with secondary γ relaxation
The Journal of Chemical Physics **123**, 014907 (2005); 10.1063/1.1948372

Dynamics of Polymer Molecules in Dilute Solution: Viscoelasticity, Flow Birefringence and Dielectric Loss
The Journal of Chemical Physics **24**, 269 (1956); 10.1063/1.1742462

PHYSICS TODAY
WHITEPAPERS

ADVANCED LIGHT CURE ADHESIVES

Take a closer look at what these environmentally friendly adhesive systems can do

READ NOW

PRESENTED BY
MASTERBOND
ADHESIVES | SEALANTS | COATINGS

Spatial correlations in polycarbonates: Neutron scattering and simulation

J. Eilhard and A. Zirkel
Institut für Festkörperforschung, Forschungszentrum Jülich, D-52425 Jülich, Germany

W. Tschöp, O. Hahn, and K. Kremer
Max-Planck-Institut für Polymerforschung, D-55021 Mainz, Germany

O. Schärpf
Institut Laue-Langevin, F-38042 Grenoble, France

D. Richter and U. Buchenau
Institut für Festkörperforschung, Forschungszentrum Jülich, D-52425 Jülich, Germany

(Received 13 July 1998; accepted 14 October 1998)

We present the results of a combined experimental (neutron scattering) and theoretical (computer simulation) effort to investigate structural properties of polycarbonate melts and glasses in the wave vector regime of $Q \leqslant 2.2$ Å^{-1}. The experimental part consists of advanced spin polarized scattering experiments, allowing us to extract the coherent scattering for protonated and deuterated samples. The simulations employ recently developed novel mapping procedures, which allow us to efficiently equilibrate complex polymer melts, thereby reproducing the experiment in much closer detail than earlier attempts. © *1999 American Institute of Physics.* [S0021-9606(99)50603-X]

I. INTRODUCTION

It is most desirable, both from a fundamental and a technological point of view, to be able to relate the macroscopic properties of polymers to their atomistic structure. So far typical structure property relations have the character of empirical look-up tables,[1] and lack any structural (the structure of the bead liquid) or conformational (chain conformation) systematic scientific interpretation. A deeper understanding, however, is required for significant further progress.

In order to proceed in this direction, a solid knowledge of the conformational and structural properties is required. So far that knowledge is developed to a very limited extent. Scattering experiments give only information on the pair correlation functions. The detailed interpretation of the data in terms of the atomic structure needs many more or less justified assumptions. On the other hand, computer simulations give a precise insight into the atomic structure. However there one faces the problem of computer time to equilibrate samples of the necessary size, together with the open question of the quality of the classical force fields. Thus one needs the scattering experiment in order to validate the simulation.

The present paper describes such a coordinated effort, where significant methodical advances from both sides are combined into a joint effort from neutron scattering and computer simulations to elucidate the structure of a polymeric melt. The investigation extends a promising line of research to a significantly higher level.

The work centers around bisphenol A polycarbonate (BPA-PC, see Fig. 1). BPA-PC is one of the most important thermoplastic polymers because of its many technologically favorable properties. Among them, mechanical performance like high impact strength at low temperatures (down to -100 °C) and a high glass transition temperature (150 °C) is desirable, but also causes problems in processing. Chemical modifications have a rather strong influence on these properties. In, for example, the case of tetramethyl-bisphenol A polycarbonate (TMBPA-PC) one has a more brittle material with a glass transition at 200 °C, while the glass transition of TMC-PC is around 240 °C. These changes are accompanied by a significant variation in the so-called entanglement length and other relaxational quantities.

The first systematic neutron scattering investigation with differently deuterated samples of BPA-PC was done by Červinka *et al.*,[2] yielding important information on the distribution of the scattering units. These experiments, however, were done with unpolarized neutrons and did not allow one to separate the coherent and incoherent scattering for the same sample. Such a separation is only possible with polarized neutrons. Using polarized neutrons allows one to explicitly subtract the incoherent scattering from the total scattering intensity (see below), giving the coherent scattering cross section in absolute numbers. First experiments of this kind on polycarbonates (PC) were performed by Lamers *et al.*[3] using a triple-axis spectrometer with a relatively low intensity and a comparatively poor statistical accuracy of the measured scattering function.

In the present study those investigations are improved and extended significantly. We present in detail new investigations on different polycarbonates and similar polymers using spin polarized neutrons at the multidetector spectrometer D7 at the Institute Laue–Langevin in Grenoble. This spectrometer enables simultaneous measurements at 32 different Q values. Consequently, the differential cross section can be determined in a rather short time with excellent statistics, comparable to the statistics obtainable with unpolarized neutrons.

Parallel to these improvements of the scattering investigations of polycarbonates, a novel computer simulation ap-

 © 1999 American Institute of Physics

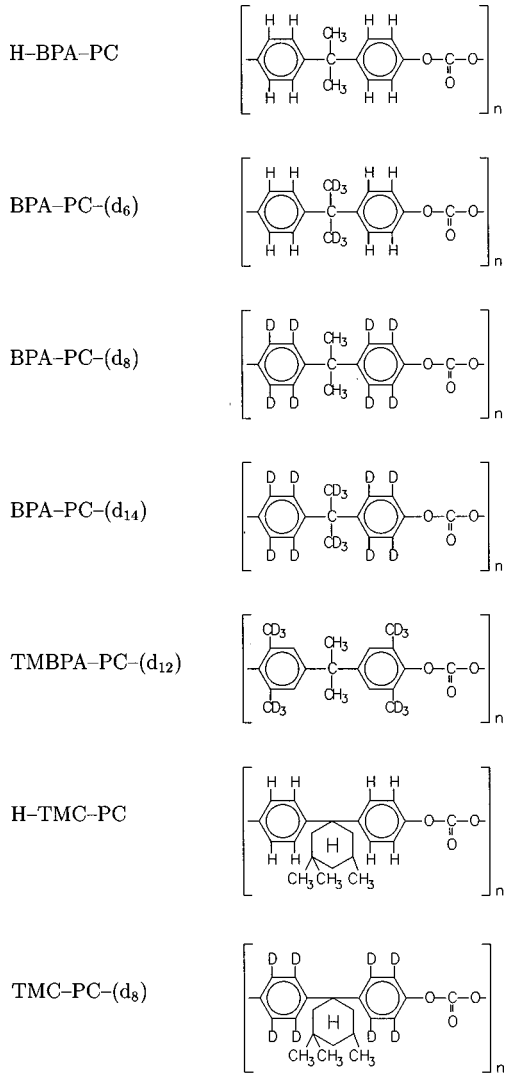

FIG. 1. Repeat units of polycarbonate samples. With the exception of TMBPA-PC, all systems are also treated in computer simulations.

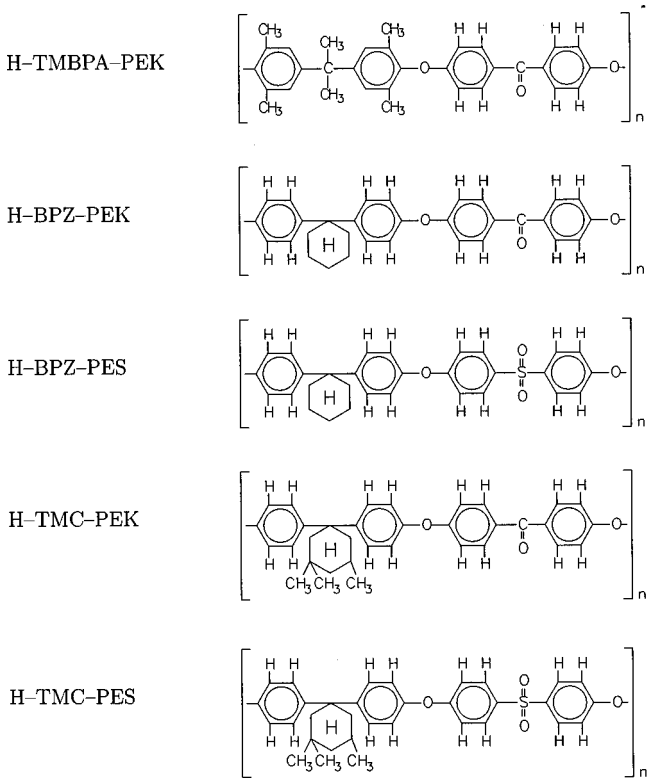

FIG. 2. Repeat units of PEK and PES samples. For these polymers only experimental data are available so far.

proach was developed to generate and analyze ''samples'' of PC of reasonable size and at experimentally accessible temperatures.[4,5] A direct brute force equilibration of such a computer simulation is not possible at present and will remain impossible for several generations of computers to come. Here a different approach is followed. A systematic procedure was introduced which coarse grains atomistic polymer models into a mesoscopic model[4] for the purpose of computer simulations. This model allows a fast and effective relaxation of polymer melts, producing overall well equilibrated conformations. The mesoscopic conformations include the atomistic structure only in an average way, but they reproduce several macroscopic properties very well. For a comparison to microscopic experiments, however, an atomistically detailed ''computer sample'' is needed. Thus the next step in the procedure is the remapping of the chemical details onto the coarse grained chains (*inverse mapping*).[5] Since the mesoscopic structure is well equilibrated, only a local equilibration is needed on the atomistic level involving motions on distances of the order of 1–2 Å at most. From the gained atomistic conformations coherent structure functions can be calculated and compared to the neutron scattering experiments. This has been done for two PC modifications.

Sections II and III describe the experimental and theoretical ansatz in more detail. Then the results of both will be presented together. Experiments on additional PC modifications are discussed in Sec. V, while Sec. VI concludes the present work with a general discussion and outlook.

II. EXPERIMENTAL METHOD AND SYSTEMS

Neutron scattering studies were performed on the following PC modifications, provided by the Bayer AG

TABLE I. Incoherent cross sections per monomer unit (in barn/sr) and sample transmissions T for the systems studied.

Sample	$\left(\frac{d\sigma}{d\Omega}\right)_{\text{inc}}$	T
H-BPA-PC	89.0	0.88
BPA-PC-(d_6)	53.3	0.77
BPA-PC-(d_8)	42.9	0.82
BPA-PC-(d_{14})	6.2	0.89
TMBPA-PC-(d_{12})	70.0	0.90
H-TMC-PC	152.6	0.68
TMC-PC-(d_8)	103.1	0.87
H-TMBPA-PEK	190.8	0.85
H-BPZ-PEK	165.3	0.73
H-TMC-PEK	203.5	0.76
H-BPZ-PES	165.3	0.78
H-TMC-PES	203.5	0.71

TABLE II. Transmissions of the four protonated BPA-PC samples.

Sample	T_P
H-BPA-PC 0.10 mm	0.88
H-BPA-PC 0.25 mm	0.77
H-BPA-PC 0.45 mm	0.58
H-BPA-PC 0.57 mm	0.49

[see Fig. 1]: protonated (further assigned as ''H-BPA-PC''), methyl group deuterated [''BPA-PC-(d_6)''], phenyl ring deuterated [''BPA-PC-(d_8)''], and perdeuterated [''BPA-PC-(d_{14})''] sample. Furthermore we studied partial deuterated TMBPA-PC-(d_{12}) (only experiment) and two different samples of trimethylcyclohexylidene polycarbonate [''H-TMC-PC'' and ''TMC-PC-(d_8)'']. The average degree of deuteration for the deuterated parts was 95%. In addition to the polycarbonate samples we studied some derivatives where ketone and sulfone groups replaced the carbonate unit, called polyetherketones and polyethersulfones, respectively (see Fig. 2).

The samples (average thickness 0.2 mm) were prepared in hollow cylindric form with a height of 50 mm and a radius of 5 mm and were put into a cylindric aluminum sample holder. To suppress thermal excitations, the samples were kept in a cryostat at an average temperature of 1.5 K.

To extract the coherent cross section, all measurements were carried out in spin-flip (SF) and non-spin-flip (NF) mode. In the first, one measures only scattered neutrons which have undergone a spin flip in the scattering process, in the second the rest which maintains its spin direction in the scattering process. We denote the momentum transfer of the scattering process by Q, the spin-flip counting rate by I^{SF} and the non-spin-flip counting rate by I^{NF}. The coherent scattering function is given by (see the Appendix)

$$\left(\frac{d\sigma}{d\Omega}\right)_{\mathrm{coh}}(Q)=\frac{2}{3}\left(\frac{d\sigma}{d\Omega}\right)_{\mathrm{inc}}\frac{I^{\mathrm{NF}}(Q)-\frac{1}{2}I^{\mathrm{SF}}(Q)}{I^{\mathrm{SF}}(Q)}. \tag{1}$$

The values of the incoherent cross section $(d\sigma/d\Omega)_{\mathrm{inc}}$ can be calculated and are given in Table I. In order to cover the full Q range, the detector positions for every measurement were changed incrementally by 1.5° three times, giving 128 different Q values for each sample in the range $0.2\ \text{Å}^{-1}\leqslant Q\leqslant 2.5\ \text{Å}^{-1}$.

Equation (1) is valid in the ideal case where one has only single scattering processes. In a real sample, one has to reckon with multiple scattering. In order to study that influence, samples of BPA-PC of four different thicknesses between 0.1 and 0.57 mm were measured. (cf. Table II). The scattering patterns of the different samples were almost identical, but with a Q-independent offset of the coherent cross section [Fig. 3(a)] which depended on the sample thickness. Beyond that no effect of the sample thickness was observed. The Q-independent offset increases with increasing sample thickness. Since only the incoherent scattering intensity is independent on Q, this offset is due to multiple incoherent scattering involving two spin flips and being detected as NF neutrons.

Thus multiple scattering results in an overestimation of the coherent scattering. This effect can be corrected by using expression (2) for the apparent coherent cross section which has to subtracted from the measured cross section:[3]

$$\left(\frac{d\sigma}{d\Omega}\right)_{\mathrm{coh}}^{\mathrm{app}}=\left(\frac{2}{3}\right)^2(1-T_P)\times\frac{\left(\frac{d\sigma}{d\Omega}\right)_{\mathrm{inc}}^2}{\left(\frac{d\sigma}{d\Omega}\right)_{\mathrm{inc}}+\left\langle\frac{d\sigma}{d\Omega}\right\rangle_{\mathrm{coh}}+\left(\frac{d\sigma}{d\Omega}\right)_{\mathrm{abs}}}. \tag{2}$$

Here $\langle d\sigma/d\Omega\rangle_{\mathrm{coh}}$ is the average coherent cross section and $(d\sigma/d\Omega)_{\mathrm{abs}}$ is the calculated absorption cross section. The subtraction procedure is applied iteratively and converges after a few steps. We obtain the same coherent cross sections for three of the investigated samples. Only in the case of the 0.6 mm sample (with a very low transmission of 49%) the correction fails [Fig. 3(b)]. Since all other samples had transmissions higher than that of the second thickest sample (Table I), the multiple scattering correction procedure could be applied.

For a crude evaluation, the measured cross section can be used directly to deduce particle–particle correlation functions. The wave number Q at the peaks at the cross section is approximately related to a distance D between different atoms or groups of atoms by

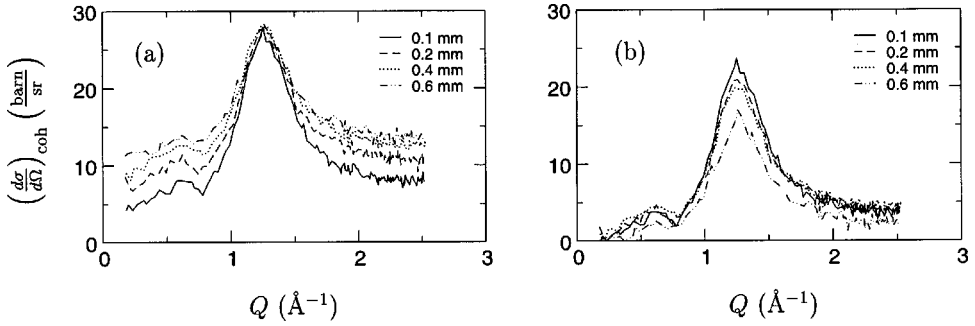

FIG. 3. Coherent cross sections of BPA-PC (a) before and (b) after the multiple scattering correction.

$$D=\frac{2\pi}{Q}. \tag{3}$$

For a peak at wave number Q, the width ΔQ is a measure of the correlation length ξ of such a local arrangement,

$$\xi=\frac{2\pi}{\Delta Q}. \tag{4}$$

Equations (3) and (4) provide helpful means for the interpretation of the structure functions.

In addition to these equations, one can use arguments based on the atomic scattering lengths in Table V to obtain structural information from the measured $S(Q)$. One rather general argument of that kind holds for the protonated polymers investigated in our work. It is the following: The scattering length of hydrogen is the only negative one for all participating atoms, while the carbon and oxygen scattering lengths are positive. Thus one has a positively scattering backbone with a surrounding shell of negative scattering density. Considering the tendency of neighboring chains to lie parallel to each other, that scattering density distribution tends to give a large contrast to the correlation between different chains for fully protonated samples, because the interference between the two different positively scattering backbones is enhanced by the negatively scattering hydrogens in between. In fact, in all the examples reported below, the fully protonated polymers exhibit a clearcut diffraction peak between 1 and 2 Å^{-1}, where one expects the interchain correlation, while the deuterated samples show more and less pronounced peaks in that region, probably because they are much more strongly influenced by intrachain correlations. We will see later that the simulations support that point of view.

Beyond this it is rather difficult to identify individual atomic groups which contribute to a specific peak on the basis of the cross sections alone. If one wants to go further, one has to use some kind of modeling. At this point, simulations come into play, since they are in principle able to provide the full structural information.

III. COMPUTER SIMULATION APPROACH

To relate simulation data directly to scattering experiments and extend their interpretation, one has to calculate the measured scattering functions. This requires the generation of well equilibrated ''computer samples'' with all atomistic details. While the simulation in principle yields many additional quantities, we focus here on the scattering.

To achieve a good equilibration, a new recently developed two-step procedure[4,5] is applied. First the chains with the full atomistic details are numerically renormalized onto a coarse grained mesoscopic model (''mapping step''). A melt of coarse grained chains is then equilibrated. This is possible due to a significant gain in simulation speed $[O(10^4)]$ compared to atomistic simulations. Then we perform the inverse step (''*Inverse mapping*'') and reintroduce the full atomistic details. After that a local equilibration with a short simulation run is performed. This only alters the atom positions on very short scales [O(1 Å)]. These so generated systems are used to calculate the cross sections, which can be compared to experiment.

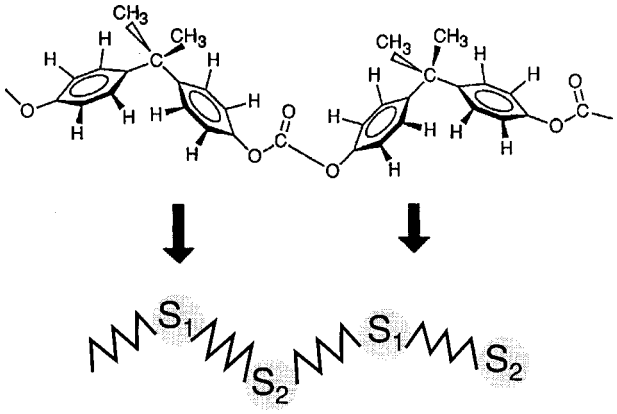

FIG. 4. Illustration of the 1:2 mapping of BPA-PC. The center of the sphere S_1 is given by the geometrical center of the isopropylidene group (CH_3–C–CH_3), while S_2 corresponds to the geometrical center of the carbonate group.

A. The mapping procedure

The first step coarse graining[4] renormalizes the intrachain interactions toward a coarser level. For BPA-PC as well as for TMC-PC we map one chemical repeat unit onto two model monomers (mapping ratio 1:2, see Fig. 4). These coarse grained monomers are chosen in such a way that they can be identified with specific chemical groups of the polymer. In the case of BPA-PC the two coarse grained monomers represent the carbonate group and the isopropyledene group. For modeling TMC-PC the isopropyledene group has to be substituted by the decorated cyclohexane ring. For the resulting coarse grained chain, only four relevant effective potentials have to be considered: the bond length potential between two adjacent model monomers, two alternating bond angle potentials, and one torsional potential. All the much more complicated interactions along the chain are renormalized into these four intramolecular interactions.

The determination of the effective potentials is done in the following way: One calculates a statistical ensemble of the full atomistic chain in free space, using interactions derived by *ab initio* quantum chemistry calculations. With the above mapping, one then finds the distribution functions of bond lengths and angles defined by the monomers of the coarse grained chain. On the basis of these probability distributions, the potential within a coarse grained chain can be computed without any free parameter. For details see Ref. 4.

In addition to these intramolecular interactions within the chain, the intermolecular interactions (e.g., excluded volume) are taken into account via a purely repulsive Lenard-Jones interaction. The density of the systems is varied with the temperature and scaled according to the thermal expension given by experimental data. From this model, the global properties like the end-to-end distance of the polycarbonate chains can be calculated. Tables III and IV give the simulation results for the end-to-end distance R and the gyration radius R_G for a chain with 20 (e.g., $M=2530$) and 60 (e.g.,

TABLE III. R^2 and R_G^2 for $N=20$ from simulation for BPA-PC (in Å^2), error 1.5%.

T	600 K	800 K	1000 K
R^2	328	322	321
R_G^2	57	53	52

$M=7590$) simulation model monomers for BPA-PC.

Though the expected asymptotic ratio of $\langle R^2\rangle/\langle R_G^2\rangle=6$ is not fulfilled exactly, data for $N=60$ ($\approx$30 chemical repeat units) are reasonably close to this asymptotic limit. One usually characterizes chains in a melt by their ratio $\langle R_G^2\rangle/N$. For $T=300$ K, in the glass regime, neutron scattering experiments performed by Richter *et al.*[6] quote $\langle R^2\rangle/N=37$ Å^2. Our simulations yield $\langle R^2\rangle/N=35$ Å^2 at $T=600$ K and $N=60$, which is in excellent agreement with the experimental data at even lower temperatures. The chains expand at lower temperature, so the simulation value is even closer to the experimental data when extrapolated to T_G. The good agreement shows the success of the mapping procedure as far as the large scale chain properties are concerned.

One can go a step further and show that also more microscopic details are still reasonably well taken into account by the coarse-grained chain. An interesting local aspect of the BPA-PC chain is the amount of the *trans* and *cis* conformations of BPA-PC. Along the backbone of the full atomistic chain, at the carbonate group, one has two torsional bonds, each of which can be in a *cis* or a *trans* conformation. For both together, one can have either a *trans–trans* or a *trans–cis* (or *cis–trans*, respectively) conformation. The *cis–cis* conformation is forbidden because of overlapping phenyl rings. The mapping transfers only part of this information into the coarse grained model. There, it appears as a broad double-peak structure in the bond angle distribution at the monomer S_2 (see Fig. 4). The amount of *trans–cis* isomers can be still roughly estimated by considering the area under the peaks of the angle distribution at different temperatures T.[5] But there is no exact correspondence between the peaks and the conformations possible on this level, as the two peaks overlap. That is understandable, since several microstates with different conformation are mapped onto one coarse grained state. A more exact estimate of the *cis–trans* conformation ratio can only be given after reintroducing the full chemistry. In the case of BPA-PC this probably leads to an overestimation of the *trans–cis* states. In Fig. 5 the percentage of *trans–cis* conformations determined from the coarse grained chains is shown as a function of the temperature. For the temperature of $T=600$ K the *trans–cis* percentage for the full atomistic chains after the inverse mapping (see below) is also shown. Note that these numbers strongly

TABLE IV. R^2 and R_G^2 for $N=60$ from simulation for BPA-PC (in Å^2), error 1.5%.

T	600 K	800 K	1000 K
R^2	1046	1038	1004
R_G^2	191	183	168

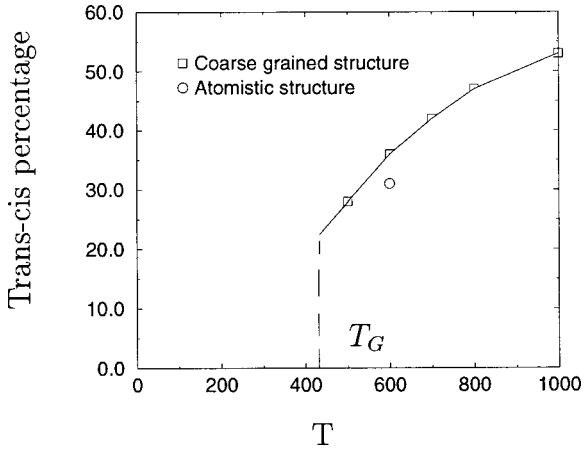

FIG. 5. Percentage of *trans–cis* isomers in the simulated melt in dependence of the temperature (BPA-PC). The values for the coarse grained chains are gained by considering the area under the peaks of the bond angle distribution at S_2. At $T=600$ K the value is also measured from the atomistic structure (after inverse mapping).

influence R_G, since the torsion is the relevant degree of freedom of the global conformation. A lower percentage of *trans–cis* isomers leads to a more stretched molecule. An extrapolation of the data toward lower temperatures suggest a *trans–cis* fraction clearly below 20% of the states of BPA-PC at around T_G, NMR experiments suggest even lower values of at most 10%.[7]

B. The inverse mapping

The second step is the remapping of the chemical details onto the coarse grained chains,[5] called *inverse mapping*. We start with an atomistic chain with the correct average bond lengths and bond angles but free torsion angles. The detailed chain is placed onto the coarse grained chain by a suitable rotation of the torsional degrees of freedom. For this the distance between the center of mass of the model monomers and the geometrical center of their corresponding atomistic group is minimized. Then in the melt the van der Waals interaction of the atoms is slowly introduced. After minimi-

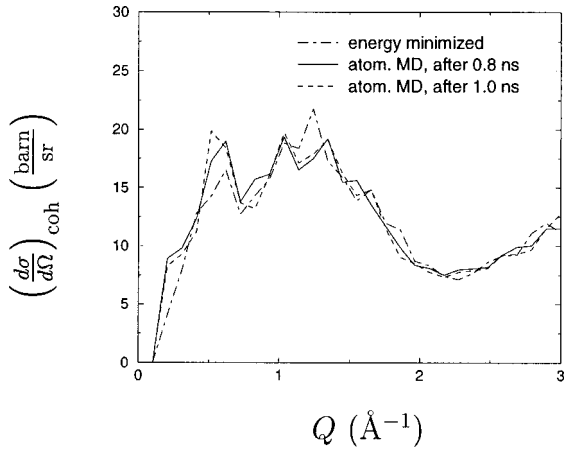

FIG. 6. Structure factor of a simulated atomistic melt of TMC-PC at different stages of the relaxation procedure: directly after the energy minimization, after a 0.8 ns long atomistic MD run, and after 1.0 ns of atomistic MD.

zation the system can be trapped in a local minimum. To overcome this problem the melt of the atomistically detailed chains is relaxed locally by molecular dynamics (MD) runs using the YASP package.[8] During the relaxation of the structures by an atomistic MD we observe a decrease in the potential energy which corresponds to a change in the microscopic structure of the samples. After a simulation time of more than 1 ns the energy converges slowly to a constant value. This also has an effect on the structure factor of the system, as shown in Fig. 6 in the case of TMC-PC for different stages of the equilibration. During this local relaxation the intensities, but not the positions of individual peaks change.

The simulation boxes contained 80 chains with a length of 10 chemical repeat units, which means systems as large as ≈30 000 atoms in the case of BPA-PC and ≈40 000 atoms for TMC-PC. The corresponding box size was $\approx 70^3$ Å^3. The coarse grained simulations were run for ≈15 μs, thus allowing for a relaxation on large length scales. After reintroducing the full chemistry, local relaxation was achieved by means of an atomistic MD of ≈200 ps.

Given the computer generated ''samples,'' we calculate the coherent structure functions

$$S(Q)=\left(\frac{d\sigma}{d\Omega}\right)_{\text{coh}}=\sum_{ij}\langle b_i\rangle\langle b_j\rangle\exp(i\mathbf{Q}\cdot(\mathbf{r}_i-\mathbf{r}_j)), \qquad (5)$$

which are compared to coherent neutron scattering data. In Eq. (5) all atoms are explicitly included with their corresponding scattering length $\langle b_j\rangle$ cf. Table V,[9] which are independent of Q. For TMC-PC the methyl groups at the cyclohexane ring were substituted by super atoms with an average scattering length. To calculate $S(Q)$ for a simulation system, one is restricted to scattering vectors Q which are commensurate with the box size L, namely

TABLE V. Scattering length for different atoms.

Atom	Scattering length (10^{-12} cm)
H	−0.3741
D	0.6674
C	0.6648
O	0.5805

$$Q_x=\frac{2\pi n_x}{L}, \quad Q_y=\frac{2\pi n_y}{L}, \quad Q_z=\frac{2\pi n_z}{L}, \qquad (6)$$

where n_x, n_y, n_z are integer numbers. Only for these discrete scattering vectors can $S(Q)$ be calculated.

IV. COMPARISON OF SIMULATION AND EXPERIMENT

Figure 7 compares simulation and experiment for the differently deuterated BPA-PC samples. First we consider the experimental results (the circles in Fig. 7). The *protonated* H-BPA-PC [Fig. 7(a)] basically shows an ''amorphous halo'' with a maximum at $Q=1.27$ Å^{-1} and a width $\Delta=0.23$ Å^{-1}. Following the argument at the end of Sec. III, we identify this amorphous halo with the correlation between different neighboring chains, resulting in an average chain distance of 4.9 Å. Taking the peak width as indicative of the persistence of short range order a correlation length $\xi=27.6$ Å can be deduced. Furthermore there is a second maximum of lower intensity at $Q=0.56$ Å^{-1}. By ''amorphous cell'' computer simulation this maximum was related earlier to the correlation of consecutive carbonate groups along one chain.[10] Thus we get an average monomer extension of $2\pi/0.56$ Å$^{-1}\approx 11.2$ Å.

In the case of *methyl group deuterated* BPA-PC-(d_6) [Fig. 7(b)] the peak of the amorphous halo is slightly shifted to a bigger Q value (1.32 Å^{-1}) and broadened in comparison

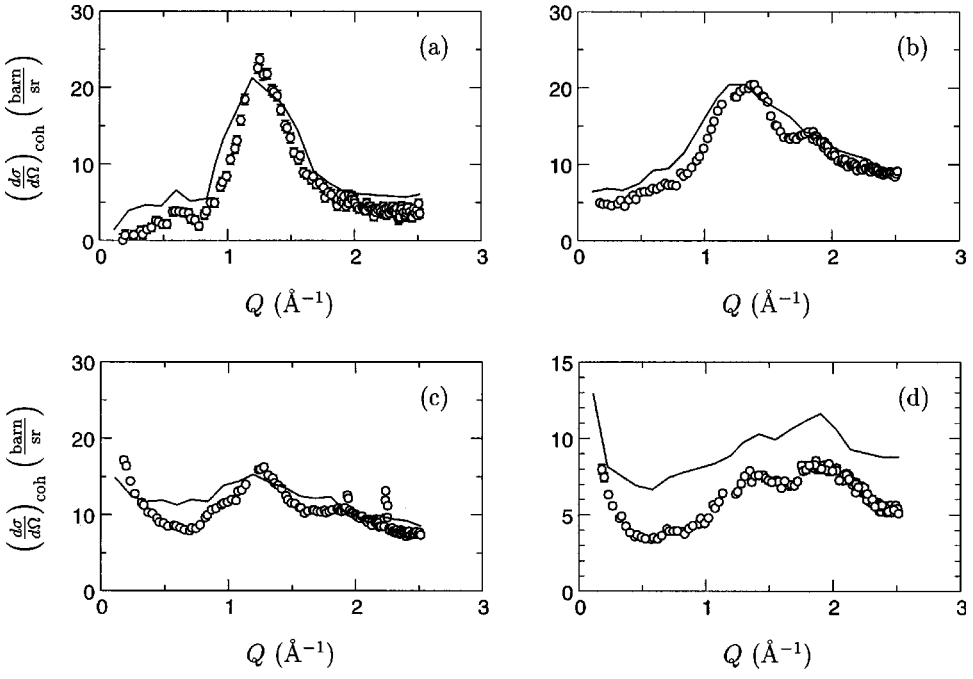

FIG. 7. Structure factor of BPA-PC from simulation and neutron scattering (a) fully protonated, (b) methyl group deuterated, (c) phenyl rings deuterated, (d) fully deuterated.

to the protonated sample. This suggests that additional correlations are superimposed on the amorphous halo. Furthermore there is a second maximum at $Q=1.80\ \text{Å}^{-1}$.

In the coherent cross section of *phenyl ring deuterated* BPA-PC-(d_8) [Fig. 7(c)] we find the amorphous halo at the same Q value as in the fully protonated case. Obviously this sample contains partially crystallized regions, since two Bragg peaks at $Q=1.94\ \text{Å}^{-1}$ and $Q=2.24\ \text{Å}^{-1}$ were found. In the rhombic unit cell of the partial crystalline BPA-PC these peaks would correspond to the reflections (130) respectively (315), but no lower order reflections were measured. Therefore these peaks cannot be due to crystalline polycarbonate. We suppose that the sample contains a small amount of crystallized solvent. There is a remarkable increase in the cross section at small Q values.

Such an intensity at low Q is also found in the cross section of *perdeuterated* BPA-PC-(d_{14}) [Fig. 7(d)]. We will comment on this small angle scattering in more detail below. Here we just note that the average scattering density, which determines the intensity of the scattering from large-scale inhomogeneities of the samples, increases with increasing deuteration and is nearly zero in the fully protonated sample. That explains why one only sees that intensity at small Q for the deuterated samples and not for the protonated sample.

In the perdeuterated case, the amorphous halo is transformed into two shallow peaks of almost equal intensity at $Q=1.42\ \text{Å}^{-1}$ and $Q=1.81\ \text{Å}^{-1}$. The peak height in comparison to BPA-PC-(d_6) is smaller by a factor of 2, indicating a much reduced intra- and intermolecular contrast as compared to the hydrogen-containing compounds.

In Fig. 7 the results for the simulation (lines) of BPA-PC are also shown together with the corresponding data from neutron scattering. The general agreement is much better than in earlier comparisons of model and experiment,[10] showing the sizable improvement of the simulation by the inverse mapping technique.

Figure 7(a) shows the comparison between the experimental data and the results from our simulation for fully protonated BPA-PC. The inspection of the underlying conformations essentially confirms the explanation of the peaks given for the experimental data. Both structure functions for the protonated version show an ''amorphous halo'' at $Q\approx1.2\ \text{Å}^{-1}$, which is in fact due to the correlation of adjacent chains. Thus the simulations corroborate the scattering density argument given at the end of Sec. III.

Another peak about $Q\approx0.6\ \text{Å}^{-1}$ can be identified with consecutive atom groups within a chain. This peak is mainly caused by the correlation between the carbonate groups, but also the isopropyledene has some influence on it. The conclusion parallels the one given earlier by Lamers *et al.*,[10] who evaluated structure functions from amorphous cell simulations. The amorphous cell approach constructs the chains in the melt by a RIS scheme, without a thermalization of the melt.[11] While the experiments give a correlation length of the monomer liquid of about 28 Å, the simulations give a slightly smaller value from the cross section. We can however go back to the coarse grained simulations.[4] There the particle–particle radial distribution $g(r)$ for both intracorrelations and intercorrelations shows structure out to ≈25 Å,

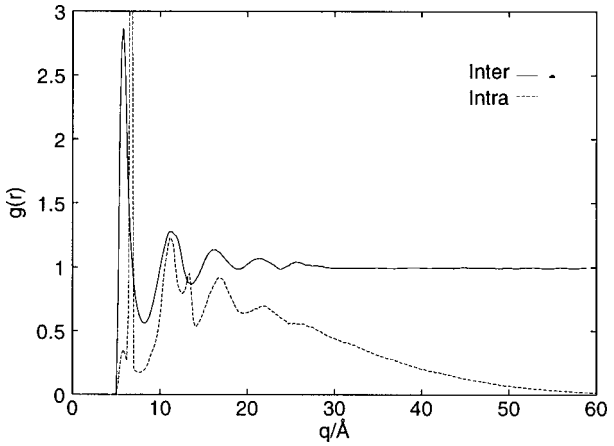

FIG. 8. Pair correlation function of BPA-PC within coarse grained chains ($T=500$ K).

as shown in Fig. 8. In Fig. 7(b) the methyl group deuterated version of BPA-PC is shown. The simulation data closely follow the experimental data. The only difference shows up at high Q, where the small peak at $Q=1.8$ Å is missing. This is possibly due to the fact that the simulations are performed at temperature $T=600$ K, while the experiments represent a quenched state at 1.5 K.

In a similar way the results of the experiment and simulations coincide for the phenyl ring deuterated BPA-PC [Fig. 7(c)]. The simulations also show an increase for low Q, meaning that there are inhomogenities in the sample exceeding the length scale of tested here (The wave vector corresponding to the size of the simulation box is $q=0.09\ \text{Å}^{-1}$). However, the visualization of slices of the simulation box did not show pronounced ''holes'' in the melt, which could be related to this increase. In fact, since the increase is *not* present in all the differently deuterated BPA-PC samples, it seems rather to indicate a correlation of certain atom groups over long distances. This certainly requires a more thorough investigation with simulations of larger systems. As expected, the simulation does not show the two Bragg peaks at $Q=1.94$ and 2.24 Å thus confirming their interpretation as an artefact of the experiment.

For the fully deuterated system, while the simulation reproduces the shape of the experimental $S(Q)$ in full detail, the overall amplitude is different. To check the simulations we evaluated the average cross section for large Q ($Q>10\ \text{Å}^{-1}$). There one should recover data with a cross section that corresponds to the mean square scattering length in the system. The program fulfills this requirement. We also checked the experiment, to see whether the difference was due to a trivial mistake or an overcorrection, but we were not able to find any reason. Thus the discrepancy is not understood as yet. A lower degree of deuteration in the calculation (within the error limits of the chemical analysis of the measured samples) slightly improves the situation, but cannot explain the difference completely (see also the discussion of TMC-PC below).

In contrast to BPA-PC the measurement of two variants of TMC-PC gave two completely different cross sections for the protonated and for the phenylene ring deuterated sample.

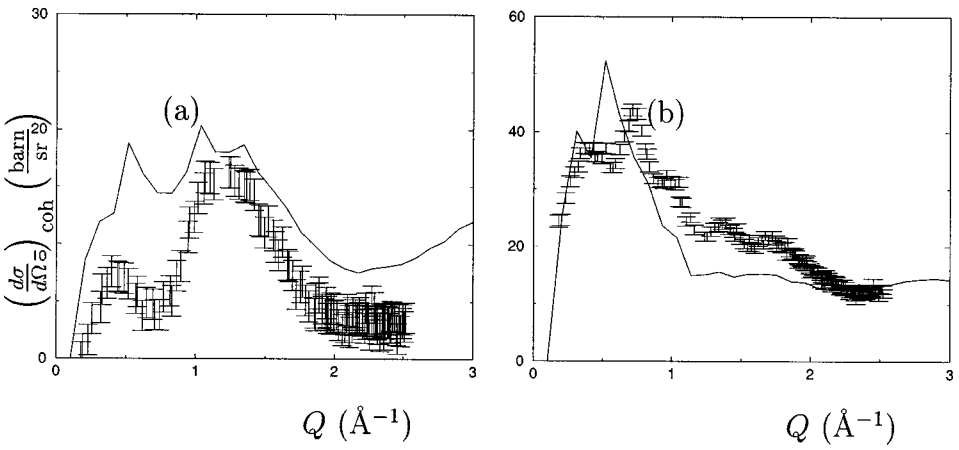

FIG. 9. Structure factor of TMC-PC from simulation (the solid line) and neutron scattering (symbols): (a) fully protonated, (b) phenyl rings deuterated.

The H-TMC-PC [Fig. 9(a)] has the amorphous halo at $Q=1.23\ Å^{-1}$ and a second maximum at $Q=0.42\ Å^{-1}$. From the halo we can determine an average chain distance of $D=5.1$ Å and a correlation length of $\xi=18.8$ Å. Obviously the chains in TMC-PC are slightly less densely packed than in BPA-PC, caused by the larger spatial extension of the cyclohexylidene ring, but also less correlated.

The cross section of TMC-PC-(d_8) shows the same low Q peak as the protonated sample, but the amorphous halo is broadened and superimposed by additional correlations [Fig. 9(b)], in particular a feature at $Q=0.8\ Å^{-1}$, in a Q range where the cross section of H-TMC-PC has a minimum. If we interpret the peak at $Q=0.42\ Å^{-1}$ in analogy to the first peak in the cross section of H-BPA-PC as the correlation of two consecutive carbonate groups, one arrives at an average monomer extension of 15.7 Å for TMC-PC. In light of the simulation results and quantum chemical calculations of a single chain, this interpretion of the experimental data seems questionable. As we will see below, the model calculations suggest a different interpretation, though still in terms of a correlation within one polymer chain.

In Fig. 9 the structure functions of TMC-PC from the simulation are shown as lines. The simulation in that case is not fully atomistic, because the united atom (UA) representation was chosen to represent the methyl group in the simulation. The corresponding scattering length is given by

$$b(CH_3)=b(C)+3b(H)=-4.575\times10^{-12}\ \text{cm} \qquad (7)$$

using the values given in Table V. For protonated TMC-PC [Fig. 9(a)] we see in simulation and experiment the same general structure with two peaks, but the first peak is much higher in the simulation and both peaks are slightly shifted. Nevertheless, the agreement is still good enough to justify a confidence in the simulation results.

The same holds for phenyl ring deuterated TMC-PC [Fig. 9(b)]. The overall shape of both curves is quite similar, but only the most pronounced peaks are reproduced in the simulation. Also, the peaks are shifted to smaller Q values. But again one feels that the simulation reflects the same atomic correlations as the neutron experiment. In consequence, one can use the simulation to check the earlier interpretation of the neutron scattering data, namely that the peak with the lowest Q value corresponds to the correlation between consecutive atom groups within a chain, while the second maximum is caused by the package of adjacent chains. As we will see, the simulations corroborate that main idea, but with a modification in detail.

The detail which has to be modified concerns the atomic group responsible for the peak at $\approx0.5\ Å^{-1}$. The calculation of the free fully atomistic chain showed that the straightforward interpretation in terms of carbonate group correlations, parallel to the BPA-PC case, would require rather strongly changed bond angles in the TMC group. This peak is more pronounced than the corresponding one in protonated BPA-PC [Fig. 7(a)]. In the following, we begin the analysis of the peak in terms of the atomic structure by a scattering density argument.

Since the Q value of the peak corresponds to a distance of about 12 Å, we are allowed to coarsen the view on the melt, considering groups of atoms instead of single atoms. We begin by joining each hydrogen to its carbon atom, thus using a ''united atom'' representation. We then subdivide the TMC-PC monomer into three groups: The TMC group with the cyclohexane ring, the carbonate group, and the phenyl group.

We then have the following:

(1) the TMC group C_9H_{16} with the cyclohexane ring consisting of nine united atoms with an average scattering length of $b=0.166\times10^{-12}$ cm,
(2) the carbonate CO_3 group consisting of four united atoms with an average scattering length of $b=0.602\times10^{-12}$ cm,
(3) the phenyl group C_6H_4 consisting of six united atoms with an average scattering length of $b=0.336\times10^{-12}$ cm.

In this counting, the average scattering length per united atom for the whole monomer $\langle b\rangle_{monomer}$ equals 0.415. Since b_{phenyl} is close to $\langle b\rangle_{monomer}$, the phenyl rings are essentially ''invisible.'' The carbonate group is a ''high b'' scatterer, while the cyclohexane ring acts as ''scattering hole.'' Since the spatial extension of the TMC group is much larger than that of the carbonate, the cyclohexane ring should mainly be responsible for the peak at $\approx0.5\ Å^{-1}$.

The simulation allows us to check this hypothesis by modification of scattering lengths. By varying the scattering

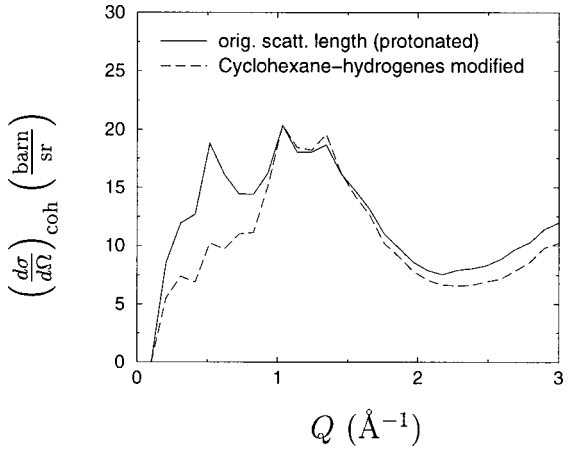

FIG. 10. Impact of modified scattering lengths for cyclohexane hydrogenes on the structure factor of TMC-PC. The peak at $\approx 0.5\ \mathrm{Å}^{-1}$ present in the simulated structure factor of Fig. 11(a) diminishes, when the natural scattering lengths of the cyclohexane-hydrogens are scaled by a factor 0.5.

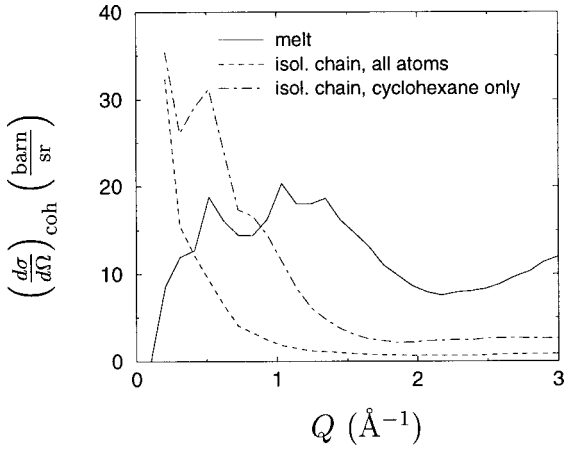

FIG. 11. Form factor of an isolated TMC-PC chain. The case where all scattering lengths are set to the same value ''1'' is compared to the case where only the TMC atoms are set to ''1'' and all other atoms to ''0.'' The latter structure factor reveals a peak, which is located at the same Q value as the peak in the structure factor of the melt. (Remark: The structure factors of the isolated chains have been scaled by a factor of 8 and 2, respectively). Note that the absolute values of the single chain form factor and of the scattering function of the whole system cannot be compared, since the normalization is fundamentally different! One can only relate positions of peaks for $2\pi/R_G \ll Q$. The structure functions of the isolated chains were also computed with periodic boundary conditions in the box.

length in the simulation one can emphasize the correlation between special group or set a homogenous background. As a test, the cyclohexane ring should become invisible, if we increase its total scattering length. In order to do that, we attributed the cyclohexane hydrogens half the b of a physical H, i.e., $-0.187\,05\times10^{-12}$ cm. The result is shown in Fig. 10, the peak is strongly diminished. On the other hand, if we shift the average $\langle b\rangle_{\mathrm{monomer}}$ to higher values (with the TMC groups still building holes), the peak should become more pronounced. This is the case for phenyl-deuterated TMC-PC, which explains the shape of the corresponding structure factor shown in Fig. 9(b).

The position of the TMC peak corresponds to a distance of $\approx$12 Å. Since the TMC group was also chosen to be represented by a coarse grained monomer in the melt simulations, one can determine the TMC–TMC distance from the calculations for the coarse grained chain. The peak position at $Q=0.42$ is in fact compatible with the extension of a chemical repeat unit, which supports the explanation in terms of intrachain correlations. This can be checked by a calculation of the structure factor for an individual fully atomistic chain of the melt after the inverse mapping. For this purpose, one first sets the scattering lengths of all atoms to the same value ''1.'' As depicted in Fig. 11, the calculated curve shows the typical $S(Q)\approx Q^{-2}$ behavior. When all atoms except those belonging to the TMC group are made invisible by setting the corresponding scattering lengths to ''0,'' a pronounced peak appears at $\approx 0.5\ \mathrm{Å}^{-1}$. This shows again that the peak observed in the melt simulation can indeed be identified with the correlation between successive TMC groups within the same chain.

Although for protonated TMC-PC the simulated $S(Q)$ shown in Fig. 9(a) resembles the shape of the experimentally determined $S(Q)$, there seems to be a constant offset. In order to exclude the possibility that this offset is a consequence of incorrect scattering lengths used in the simulation, the scattering cross section was calculated up to high Q values, where it should approach the constant value

$$\frac{d\sigma}{d\Omega}(Q\to\infty)=\sum_i b_i^2=14.0\ \ \mathrm{b/sr}. \tag{8}$$

It turns out that $S(Q)$ becomes essentially constant for $Q>20\ \mathrm{Å}^{-1}$, with $\sigma/\Omega(Q)=12.1$ b/sr. The difference of 1.9 b/sr is due to modeling the methyl groups as united atoms with a b determined by coherent summation [cf. Eq. (7), correct for small Q], while Eq. (8) means incoherent summation. Furthermore, since the structure factor for deuterated TMC-PC [Fig. 9(b)] does not deviate systematically from the experimental one the reason for the observed offset remains unclear.

V. ADDITIONAL NEUTRON RESULTS

In the neutron experiment, several additional polymers with a close structural relation to the polycarbonates were measured. The first of these was in fact a polycarbonate which was not considered in the simulation, namely TMBPA-PC (d_{12}). The cross section of TMBPA-PC-(d_{12}) shows two maxima at $Q=0.56\ \mathrm{Å}^{-1}$ and $Q=1.45\ \mathrm{Å}^{-1}$, resulting in correlation lengths of 11.2 and 4.3 Å, respectively (Fig. 12).

In addition to the measurements on the polycarbonates we investigated the structure factors of some modifications where ketone and sulfone groups replaced the carbonate unit (Fig. 13). These samples were fully protonated and we expect to see mainly the amorphous halo in the cross sections. Thus we can determine the influence of these groups on the average chain distance.

The cross sections of TMBPA-PEK, BPZ-PEK and BPZ-PES indeed show only the amorphous halo, whereas in the cross sections of TMC-PEK and TMC-PES there is a second maximum. In comparison to the TMC-PC sample the

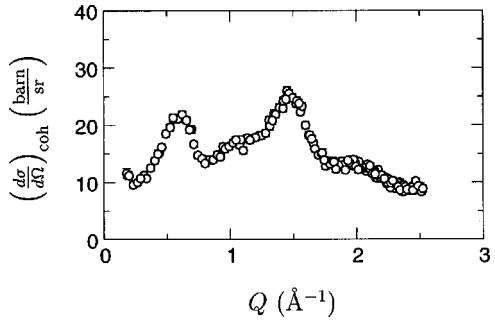

FIG. 12. Coherent scattering cross sections of TMBPA-PC.

first peak is shifted to a lower Q value (0.37 vs. 0.42 Å^{-1}). If we interpret it as the correlation of the methyl groups at two consecutive cyclohexylidene rings, we find an average monomer length of 17 Å for the PEK and PES samples, and 15 Å for the TMC-PC sample. This interpretation can be justified by comparison with the cross sections of the BPZ samples where no such maximum occurs. The only difference in the monomers are the additional methyl groups in the case of the TMC samples, so that the second maximum must be caused by these groups. A more detailed analysis with the aid of computer simulations certainly would be desirable.

TABLE VI. Parameters of the amorphous halo for the protonated samples. The values in parentheses are the results of the simulation (for BPA-PC and TMC-PC only).

Sample	Q_0(Å^{-1})	ΔQ(Å^{-1})	d(Å)	ξ(Å)
BPA-PC	1.27	0.23	4.93	27.6
	(1.21)	(0.28)	(5.19)	(22.43)
TMBPA-PC[a]	1.05	0.24	5.96	26.3
BPZ-PC[a]	1.26	0.27	4.98	23.1
TMC-PC	1.23	0.33	5.12	18.8
	(1.20)	⋯	(5.23)	⋯
TMBPA-PEK	1.14	0.30	5.49	21.2
BPZ-PEK	1.30	0.26	4.82	24.6
TMC-PEK	1.27	0.31	4.93	20.3
BPZ-PES	1.30	0.27	4.85	22.9
TMC-PES	1.27	0.32	4.93	19.9

[a]Reference 12.

VI. GENERAL DISCUSSION AND CONCLUSION

As already mentioned (cf. sec. IV), the amorphous halo provides information about the average chain distances D in a sample. Table VI summarizes the parameters of the halo for all measured protonated samples. It further includes the results for two samples (TMBPA-PC and BPZ-PC) studied

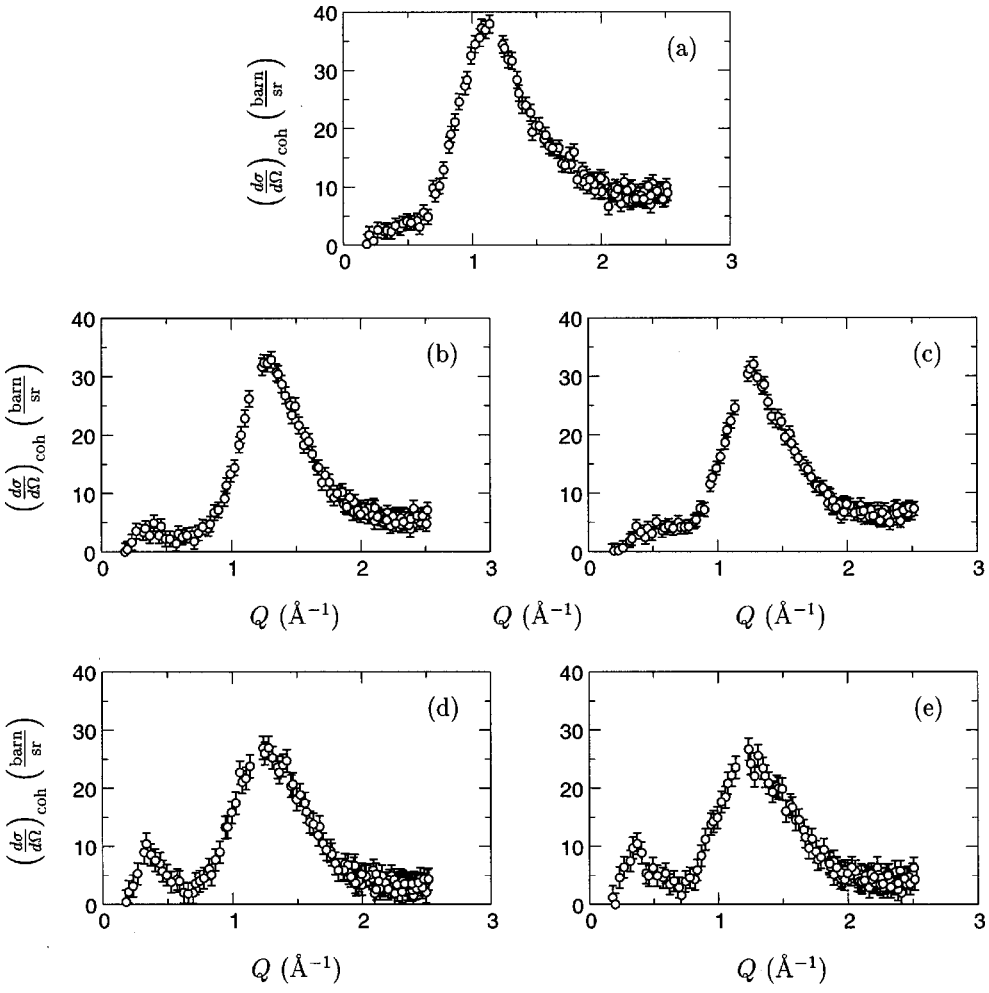

FIG. 13. Coherent scattering cross sections of (a) H-TMBPA-PEK, (b) H-BPZ-PEK, (c) H-BPZ-PES, (d) H-TMC-PEK, and (e) H-TMC-PES.

earlier by Lamers.[12] It is obvious that the average chain distance of the polycarbonates increases in the sequence BPA→BPZ→TMC→TMBPA. This can be understood qualitatively in terms of the increasing bulkiness of the monomeric structures.

In comparison to the PC samples, the chain distance of the PEK and PES samples is reduced. The more flexible ketone and sulfone groups lead to a more close packing of the chains.

The main result of this paper is a detailed agreement between neutron scattering measurements of polycarbonates and the results from computer modeling of these polymer melts with a new mapping procedure, to an extent which has never been achieved before and which demonstrates sizable progress in polymer simulation by the inverse mapping technique. An astonishing feature found both in experiment and simulation is the rise of $S(Q)$ toward small Q in BPA-PC, indicating the existence of large-scale inhomogeneities in that polymer, which seem to be absent in TMC-PC. The understanding of that result requires further investigation.

In order to understand the macroscopic properties of different polymeric systems it is important to determine the short-range correlations and microscopic structure of polymer melts. By means of the spin polarized analysis of neutron scattering experiments the coherent cross section can be determined very accurately. On the other hand it is tremendously helpful for the understanding of the structure of polymeric systems and the development of new materials to be able to model these systems. The comparison to experiment shows that the inverse mapping method is able to reproduce the microscopic structure of polymer melts in detail. It further enables an interpretation of the experimental data by extracting structural data from the simulation, thus providing a much better understanding of the experimental data.

ACKNOWLEDGMENTS

This work was supported by the BMBF under Grant Nos. 03 M 4070 8, 03 N 8008 E and by the Bayer Corp. We especially thank the other project partners [the group of K. Binder (Mainz), the group of D. W. Heermann (Heidelberg), the group of U. Suter (Zürich), and the polymer physics group of the Bayer Corp.] for many helpful discussions and fruitful collaboration. We also thank F. Müller-Plathe for discussions and the YASP packages.

APPENDIX: NEUTRON SCATTERING

For elastic scattering of neutrons the cross section is given by

$$\frac{d\sigma}{d\Omega}=\sum_{ij}\langle b_i b_j\rangle\exp(i\mathbf{Q}\cdot(\mathbf{r}_i-\mathbf{r}_j)). \tag{A1}$$

The scattering lengths b_i and b_j depend on the nuclei and their spin orientation, and whether or not the neutron spin is flipped in the scattering process. The average value can be written as

$$\langle b_i b_j\rangle=\langle b_i\rangle\langle b_j\rangle+\delta_{ij}(\langle b_i^2\rangle-\langle b_i\rangle^2). \tag{A2}$$

The brackets $\langle\cdots\rangle$ denote the average over different spin orientations of the nuclei. Inserted in Eq. (A1) one obtains

$$\frac{d\sigma}{d\Omega}=\sum_{ij}\langle b_i\rangle\langle b_j\rangle\exp(i\mathbf{Q}\cdot(\mathbf{r}_i-\mathbf{r}_j))+\sum_i(\langle b_i^2\rangle-\langle b_i\rangle^2), \tag{A3}$$

which means that we get a Q-dependent coherent term

$$S(\mathbf{Q})=\left(\frac{d\sigma}{d\Omega}\right)_{\mathrm{coh}}=\sum_{ij}\langle b_i\rangle\langle b_j\rangle\exp(i\mathbf{Q}\cdot(\mathbf{r}_i-\mathbf{r}_j)) \tag{A4}$$

and a Q-independent incoherent term

$$\left(\frac{d\sigma}{d\Omega}\right)_{\mathrm{inc}}=\sum_i(\langle b_i^2\rangle-\langle b_i\rangle^2). \tag{A5}$$

In the experiment the coherent scattering function can be determined by measuring separately spin-flip (SF) and non-spin-flip (NF) scattering processes using spin polarized neutrons and polarization analysis. Theoretical derivation[13] shows that the SF scattering is purely incoherent whereas NF scattering consists of the coherent scattering and one-third of the incoherent scattering:

$$\left(\frac{d\sigma}{d\Omega}\right)_{\mathrm{NF}}=\left(\frac{d\sigma}{d\Omega}\right)_{\mathrm{coh}}+\frac{1}{3}\left(\frac{d\sigma}{d\Omega}\right)_{\mathrm{inc}}, \tag{A6}$$

$$\left(\frac{d\sigma}{d\Omega}\right)_{\mathrm{SF}}=\frac{2}{3}\left(\frac{d\sigma}{d\Omega}\right)_{\mathrm{inc}}. \tag{A7}$$

After applying the data correction procedure for spin polarization measurements (i.e., background subtraction, corrections for finite flipping ratio and multiple scattering) which is described elsewhere,[14] the coherent scattering cross section is determined from

$$\left(\frac{d\sigma}{d\Omega}\right)_{\mathrm{coh}}(Q)=\frac{2}{3}\left(\frac{d\sigma}{d\Omega}\right)_{\mathrm{inc}}\frac{I^{\mathrm{NF}}(Q)-\frac{1}{2}I^{\mathrm{SF}}(Q)}{I^{\mathrm{SF}}(Q)} \tag{A8}$$

since the values of the incoherent cross-sections of the samples can be calculated. It is obvious that Eq. (A8) allows absolute calibration of the cross sections just by combining NF and SF data instead of using a sample standard. The simulations directly calculate $S(Q)$ via Eq. (12).

[1] D. W. van Krevelen and P. J. Hoftyzer, *Properties of Polymers* (Elsevier, Amsterdam, 1976).
[2] L. Červinka, E. W. Fischer, K. Hahn, B. Z. Jiang, G. P. Hellmann, and K. J. Kuhn, Polymer **28**, 1287 (1987).
[3] C. Lamers, C. Schönfeld, S. M. Shapiro, J. Batoulis, R. Timmermann, J. W. Cable, and D. Richter, Colloid Polym. Sci. **272**, 1403 (1994).
[4] W. Tschöp, K. Kremer, J. Batoulis, T. Bürger, and O. Hahn, Acta Polym. **49**, 61 (1998).
[5] W. Tschöp, K. Kremer, J. Batoulis, T. Bürger, and O. Hahn, Acta Polym. **49**, 75 (1998).
[6] J. Eilhard, Ph.D. thesis, 1996.
[7] R. R. Ernst (private communication).

[8] F. Müller-Plathe, Comput. Phys. Commun. **78**, 77 (1993).
[9] V. F. Sears, *Thermal-neutron Scattering Lengths and Cross-sections for Condensed Matter Research* (Chalk River Nuclear Laboratories, Chalk River, 1984).
[10] C. Lamers, O. Schärpf, W. Schweika, J. Batoulis, K. Sommer, and D. Richter, Physica B **180–181**, 515 (1992).
[11] U. Suter, Final report of BMBF Project No. 03M4038, 1992.
[12] C. Lamers, Ph.D. thesis, 1993.
[13] R. M. Moon, T. Riste, and W. C. Koehler, Phys. Rev. **181**, 920 (1969).
[14] O. Schärpf, B. Gabryś, and D. G. Peiffer, ILL-Report No. 90SC26T, 1990.